

Giant Molecular clouds: what are they made from, and how do they get there?

C. L. Dobbs^{*1,2,3}, J. E. Pringle⁴ and A. Burkert^{2,3†}

¹ *School of Physics, University of Exeter, Stocker Road, Exeter EX4 4QL*

² *Max-Planck-Institut für extraterrestrische Physik, Giessenbachstraße, D-85748 Garching, Germany*

³ *Universitäts-Sternwarte München, Scheinerstraße 1, D-81679 München, Germany*

⁴ *Institute of Astronomy, Madingley Road, Cambridge, CB3 0HA*

15 September 2018

ABSTRACT

We analyse the results of four simulations of isolated galaxies: two with a rigid spiral potential of fixed pattern speed, but with different degrees of star-formation induced feedback, one with an axisymmetric galactic potential and one with a ‘live’ self-gravitating stellar component. Since we use a Lagrangian method we are able to select gas that lies within giant molecular clouds (GMCs) at a particular timeframe, and to then study the properties of this gas at earlier and later times. We find that gas which forms GMCs is *not* typical of the interstellar medium at least 50 Myr before the clouds form and reaches mean densities within an order of magnitude of mean cloud densities by around 10 Myr before. The gas in GMCs takes at least 50 Myr to return to typical ISM gas after dispersal by stellar feedback, and in some cases the gas is never fully recycled. We also present a study of the two-dimensional, vertically-averaged velocity fields within the ISM. We show that the velocity fields corresponding to the shortest timescales (that is, those timescales closest to the immediate formation and dissipation of the clouds) can be readily understood in terms of the various cloud formation and dissipation mechanisms. Properties of the flow patterns can be used to distinguish the processes which drive converging flows (e.g. spiral shocks, supernovae) and thus molecular cloud formation, and we note that such properties may be detectable with future observations of nearby galaxies.

1 INTRODUCTION

Understanding how giant molecular clouds (GMCs) form is complicated by the difficulty of observing, or determining the progenitors of molecular clouds, whether they are small molecular clouds, HI clouds, or flows of HI gas. A common scenario is to assume that gas is converted from HI to molecular gas. In this case, the transitional stage may correspond to HI self absorption (HISA) (Gibson et al. 2005; Strasser et al. 2007; Gibson 2010). Though HISA is ubiquitous throughout the galaxy, it is not clear how it relates to molecular cloud formation. Another possibility is that dense GMCs form from gas which is molecular, but not forming stars (Pringle et al. 2001). In this case, it may be possible to trace the molecular gas with tracers such as HF and deuterium (Monje et al. 2011; Pagani et al. 2011). The likelihood of finding such gas depends primarily on the UV field, to determine what densities self shielding is effective, and how they compare to the densities at which star formation takes place. Pagani et al. (2011) propose that gas in nearby non-starforming dark clouds cannot have been molecular for more than 6 million years. Alternatively it may even be ob-

jects which are already forming stars, including IRDCs and ordinary molecular clouds that are the main precursors of GMCs.

A separate, but likely related question, is what is (are) the physical process(es) by which molecular clouds form. GMCs may be formed by gravitational instabilities, magnetic instabilities, thermal instabilities, colliding flows or the coalescence of smaller clouds. If GMCs form from the collisions, or coalescence, of smaller clouds (Field & Saslaw 1965; Tomisaka 1984, 1986; Kwan & Valdes 1987; Roberts & Stewart 1987), then these clouds must be either denser HI or H₂. Numerous models also hypothesise that molecular clouds form from colliding flows, in which case the initial density of the gas is usually taken to be sufficiently low that the gas is in the warm neutral (atomic) phase (Ballesteros-Paredes et al. 1999; Heitsch et al. 2006; Vázquez-Semadeni et al. 2007; Heitsch & Hartmann 2008; Hennebelle et al. 2008; Banerjee et al. 2009; Ntormousi et al. 2011; Vázquez-Semadeni et al. 2011).

Numerical simulations of galaxies have demonstrated the formation of GMCs from gravitational instabilities (Shetty & Ostriker 2006; Dobbs 2008; Tasker & Tan 2009; Dobbs et al. 2011a; Tasker 2011) and cloud-cloud collisions (Dobbs & Bonnell 2006; Tasker 2011; Dobbs et al. 2011a). Simulations of colliding flows typically cover much smaller

* E-mail: dobbs@astro.ex.ac.uk

† Max-Planck fellow

scales, e.g. 10's to 100's of parsecs, and by necessity adopt fairly simplified initial conditions, e.g. opposing flows in one direction, and a uniform initial density. The colliding flows are assumed to arise from stellar winds and/or supernovae (Koyama & Inutsuka 2000; Heitsch & Hartmann 2008; Ntormousi et al. 2011), spiral shocks (Leisawitz & Bash 1982), gravitational instabilities, or turbulence in the ISM (Ballesteros-Paredes et al. 1999). In most simulations the mechanism which is presumed to produce the flows is not modelled, one exception being Ntormousi et al. (2011) who recently simulated two supernovae whose expansion shells collide. To date though, the nature of colliding, or converging, flows has not been considered in a galactic context. On slightly larger scales, simulations have also modelled a supernova driven ISM, where density enhancements occur at the intersection of large scale velocity flows (de Avillez & Breitschwerdt 2004; Slyz et al. 2005; Joung & Mac Low 2006; Dib et al. 2006; Gressel et al. 2008). Again though, it is not clear whether, and on what size scales this picture applies to the ISM of observed galaxies, and whether it is reproduced in galactic models of the ISM.

In this paper we analyse simulations of galaxies which model GMC formation. We first investigate the density evolution of material that makes up molecular clouds. We do not specifically differentiate between atomic and molecular gas, since our results are independent of the chemical nature of the ISM, and the boundary between atomic and molecular gas. However for a typical galaxy, low density may be a proxy for atomic gas, and likewise high density ($\gtrsim 10 \text{ cm}^{-3}$) for molecular gas. We then show how the properties of velocity flows in our simulations indicate the physical processes which are controlling the dynamics of the ISM. The rest of the paper is divided as follows: in Section 2 we provide basic details of the simulations and how we carried out the analysis; in Sections 3–6 we present results for each model in turn, with a brief discussion on some higher resolution simulations in Section 7; in Sections 8 and 9 we provide some discussion in the context of theoretical models of the ISM, and our conclusions.

2 METHOD

2.1 Calculations

We use the results of four simulations for the analysis presented in this paper. These simulations are i) a galaxy with an imposed stellar potential, ii) a grand design spiral which uses a imposed spiral potential, iii) as ii) but with a higher level of feedback, and iv) a flocculent galaxy which includes a live stellar component. We refer to these calculations as ‘No spiral’, ‘Spiral 5%’, ‘Spiral 20%’ and ‘Flocculent’ respectively. With the exception of the Flocculent model, these simulations have been presented in a previous paper (Dobbs et al. 2011a). In all the calculations we used a Smoothed Particle Hydrodynamics (SPH) code. We provide the main details of the simulations below. A frame from each simulation is shown in Figure 1, at a time of 200 Myr.

The four simulations all model the ISM in an isolated galaxy, and include self gravity, heating and cooling of the ISM (Glover & Mac Low 2007), and supernovae feedback (Dobbs et al. 2011a). In the first three simulations, (de-

scribed in detail in Dobbs et al. 2011a), we use an external logarithmic potential to represent the gravity from stars and a dark matter halo. In the Spiral 5% and Spiral 20% models we also include a spiral component to the potential (Cox & Gómez 2002), which produces an $m = 4$ spiral density wave. The gas in these simulations is placed in a 10 kpc radius disc, with a surface density of $8 \text{ M}_\odot \text{ pc}^{-2}$. The mass per particle is 2500 M_\odot (using 1 million particles), thus we can only consider GMCs of mass $\gtrsim 10^5 \text{ M}_\odot$. We do however also discuss in Section 7 results from a couple of 8 million particle simulations, where we again used an imposed spiral potential.

In the Flocculent model, we set up the galaxy similarly to the isolated galaxy shown in Dobbs et al. (2010), using the mkkd95 program, which is part of the NEMO (Kuijken & Dubinski 1995). This is a publicly available program from the NEMO stellar dynamical software package (Teuben 1995). The galaxy contains 100,000 halo particles, 40,000 bulge particles, 1.1 million disc particles. Of the disc particles, 100,000 are star particles, and 1 million are gas. The gas represents 4 % of the mass of the disc, or $2 \times 10^9 \text{ M}_\odot$, so the mass per particle is 2000 M_\odot . Unlike the other calculations, which exhibit a constant surface density, the surface density of the gas in the Flocculent models falls off with radius.

In the first three models, we set a temperature threshold of 20 K, though in the Flocculent model we increased this to 50 K. We insert feedback, as described in Dobbs et al. (2011a). The supernovae feedback is included as thermal and kinetic feedback, and is added when a number of conditions are satisfied, but mainly that the density must exceed a critical value and the gas must be gravitationally bound. We determine the number of stars expected to form from the total mass of molecular gas in our gravitationally bound region. We then multiply this by a star formation efficiency parameter, ϵ and determine the number of massive stars, and therefore energy to insert in the ISM. The energy is distributed in the particles according to a snowplough solution. We take a density criterion for inserting supernovae of 1000 cm^{-3} in all the models except the flocculent galaxy, where we take 200 cm^{-3} . For the Spiral 5 %, No spiral and Flocculent models, we take $\epsilon = 0.05$, and for the Spiral 20 % model we take $\epsilon = 0.2$.

As we give momentum to the particles when we insert supernovae feedback, problems associated with overcooling are reduced. Overcooling could at most correspond to a factor of two overestimation of the efficiency parameter ϵ . However tests where we inserted purely kinetic energy, and half kinetic half thermal energy were not significantly different. Generally, the value of ϵ only provides a relative measure of the effectiveness of feedback in our calculations, its absolute value is subject to a large uncertainty reflecting not just the numerical implementation of feedback, but also for example the choice of initial mass function (IMF).

2.2 Analysis of gas density evolution and velocity flows

2.2.1 Tracing gas in GMCs

Two of the key questions we wish to answer are: Is the gas from which molecular clouds form typical or atypical ISM,

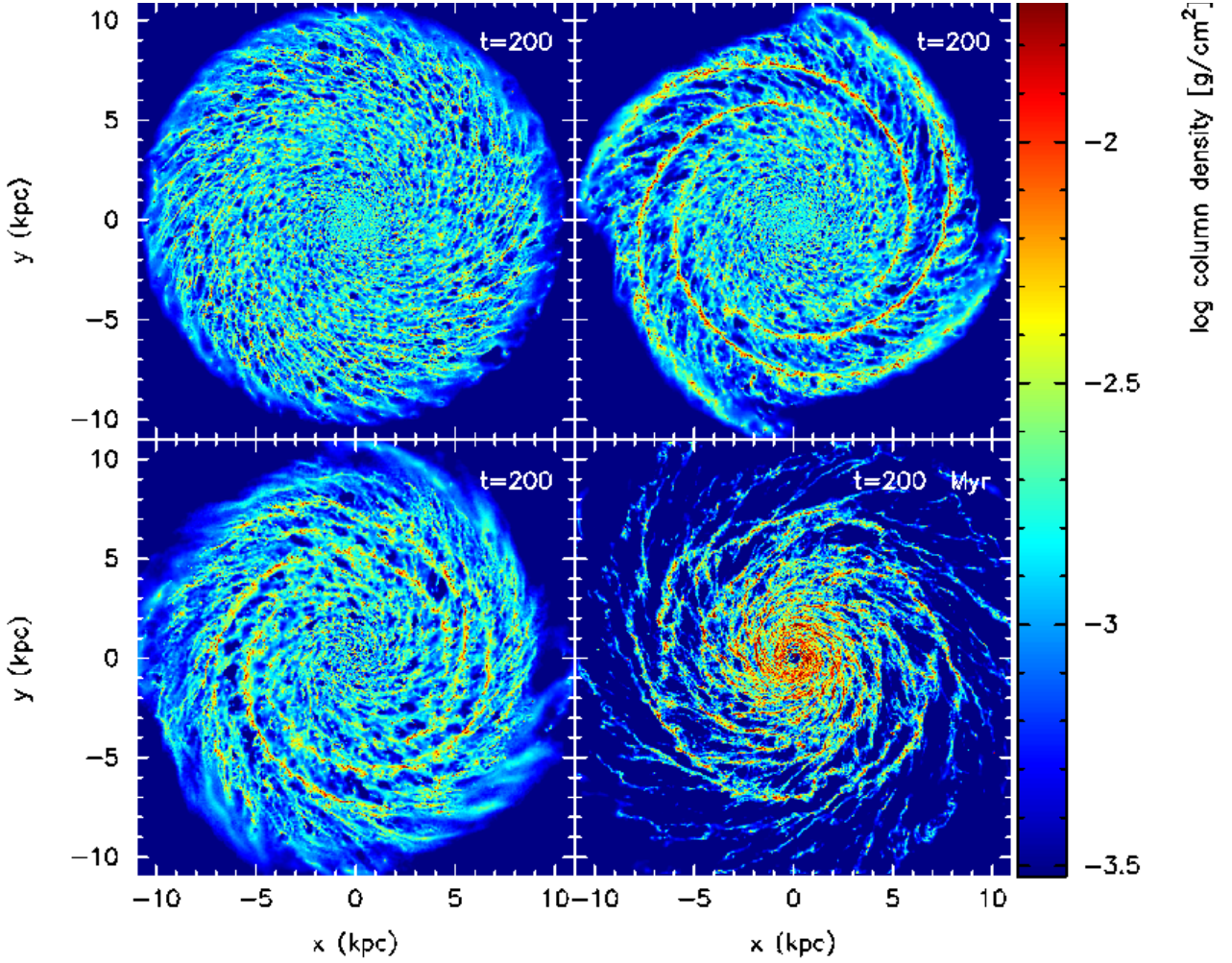


Figure 1. The gas column density is shown for the different calculations used in this paper, at a time of 200 Myr. The panels show a galaxy with a smooth potential (top left), a spiral potential (top right), a spiral potential with a strong level of feedback (lower left) and a flocculent galaxy with a live stellar component (lower right).

and, for how long is the ISM atypical? To do this we locate GMCs at a particular time frame, then we trace the particles in these clouds to earlier and to later times.

We select clouds at a time T_0 , (here 200 Myr), using a clump-finding algorithm (see Dobbs 2008). The algorithm selects cells above a given surface density threshold criterion, and then labels all cells which are adjacent as a single clump. We used cell sizes of 10 pc and 50 pc, and in both cases adopted a density criterion of $50 \text{ M}_\odot \text{ pc}^{-2}$. For the cell size of 10 pc, the clouds were required to contain at least 30 particles. For the cell size of 50 pc, the clouds naturally contained more particles, with all the clouds in the spiral potential models containing at least 100 particles. The only disadvantage with taking cells of 50 pc was that there were few clouds for some models.

For the results we present in this paper, we show the case where we used a cell size of 10 pc. In Figure 2 we show the cumulative density functions of this gas at times between $T_0 - 50 \text{ Myr}$ and T_0 for the four different simulations. In Figure 3 we show the fraction of gas above different densities versus time. In Figure 4 we study cloud dispersal and show cumulative density functions for times T_0 to $T_0 + 100 \text{ Myr}$.

Our results which used a cell size of 50 pc showed very little difference to Figures 2, 3 and 4. The only differences we noted were that there was slightly more noise, due to there being fewer clouds, and the lines on the panel for the flocculent galaxy in Figure 3 were slightly flattened. However we do not expect the results of our analysis to change. In this paper, we are considering the properties of gas that becomes especially dense. Our results are therefore primarily dependent on how the gas is organised in the galaxy, and thus the large scale gas flows, rather than the details of how the dense gas (i.e. GMCs) is selected.

2.2.2 Tracing the velocity flows

Another question we wish to address is how does gas come together to form molecular clouds? Thus we consider the velocity field of the gas. For a 2D flow field $\mathbf{u}(\mathbf{x}, t)$, the resultant local rate-of-strain tensor is

$$e_{ij} = \frac{1}{2} \left(\frac{\partial u_i}{\partial x_j} + \frac{\partial u_j}{\partial x_i} \right). \quad (1)$$

This is a symmetric tensor with two real eigenvalues λ_1 and λ_2 which have dimensions of inverse time. The sum of the eigenvalues is then the divergence of the flow,

$$\alpha = \lambda_1 + \lambda_2 = e_{ii} = \nabla \cdot \mathbf{u}. \quad (2)$$

The continuity equation

$$\frac{D\Sigma}{Dt} = -\Sigma \nabla \cdot \mathbf{u}, \quad (3)$$

where Σ is the surface density, and D/Dt is the Lagrangian derivative, then implies that the timescale on which (surface) density is changing locally is given by $1/\alpha$. Positive $\alpha > 0$ implies expansion, and negative $\alpha < 0$ implies contraction. For example $\alpha = -0.25$ corresponds to gas that contracts on a timescale of 4 Myrs. We show in Figure 5 contours of constant divergence (calculated in the plane of the disc, thus neglecting vertical motions of the gas) overplotted on column density for the different simulations. The divergence was calculated across a grid of 100 pc spacing.

We also calculate the difference between the eigenvalues

$$\beta = |\lambda_1 - \lambda_2|, \quad (4)$$

and in Figure 6 we plot each point in the flow in the $\alpha - \beta$ plane for the simulations. We highlight the points in the $\alpha - \beta$ plane corresponding to high density gas in Figure 7. As we remarked above, points with $\alpha > 0$ represent expanding regions of fluid, whereas points with $\alpha < 0$ represent contracting regions. Points which best correspond to 1D colliding flows would lie in the region $\alpha \approx -\beta$. However this region is only a small subset of the $\alpha - \beta$ plane. The axis $\beta = 0$ represents those regions where the expansion/contraction is uniform in all directions, thus we might expect points in which gravity dominates the contraction to lie close to this line for negative α . Conversely, points which exhibit negative α , but $\beta > |\alpha|$ represent regions where there is convergence in one spatial dimension, but expansion in the perpendicular direction.

3 NO SPIRAL, 5 % EFFICIENCY FEEDBACK

Figure 1 (top left) shows the structure of the galaxy which uses a stellar potential with no spiral component ('No Spiral'). The gas is dominated by structure on very small scales, likely caused by thermal and gravitational instabilities, and the stochastic nature of gas flows in the simulation. As noted in Dobbs et al. (2011a), the structure is not very realistic compared to observations, but this model provides a useful comparison. The structure and evolution are also similar to other previous calculations (Wada et al. 2000; Tasker & Tan 2009).

3.1 Density evolution

In Figure 2 (top left) we show the density distribution of material which makes up the GMCs present at the time $T = T_0 = 200$ Myr. We plot here the cumulative density distribution, so that a point on each curve represents the fraction of gas which has densities greater than n . The black (dotted) curve represents the density distribution of all of the ISM at time $T_0 - 50$ Myr.

We note first that even at time $T_0 - 50$ Myr the density

distribution of material which is going to end up in clouds at time T_0 is already considerably different to the ISM distribution. The median density of the gas is lower and the density distribution is more uniform with 80% of the gas having densities in the range $0.5 \text{ cm}^{-3} < n < 5 \text{ cm}^{-3}$, covering one order of magnitude, whereas the typical ISM has 80% in the range $0.3 \text{ cm}^{-3} < n < 30 \text{ cm}^{-3}$, covering two orders of magnitude. As we approach time T_0 the gas density distribution remains similarly narrow and steadily increases in density. The median value increases from $n \approx 0.8 \text{ cm}^{-3}$ to $n \approx 20 \text{ cm}^{-3}$ over a timescale of 40 Myr. In the final 10 Myr, however, the evolution proceeds more rapidly. The median density increases by an order of magnitude from $n \approx 20 \text{ cm}^{-3}$ to $n \approx 200 \text{ cm}^{-3}$ and the density distribution becomes much less uniform, with a larger high density tail.

In Figure 3 (top left) we plot the time dependence of the fractions of gas above various densities which is in GMCs at time T_0 . The median density of the ISM is approximately $\bar{n} \approx 2 \text{ cm}^{-3}$. At time $T_0 - 30$ Myr essentially all of the gas has density $n > 1$, but none of it has $n > 10$. From this Figure it is evident that the timescale for the appearance of the highest density gas (with $n > 100 \text{ cm}^{-3}$) is much shorter than the timescale on which the intermediate density ($n > 10 \text{ cm}^{-3}$) and lower density gas ($n > 1 \text{ cm}^{-3}$) appears. Indeed the highest density gas only starts to appear in the last 5 Myr.

From Figure 3 (top left) it is evident from the asymmetries of the various curves that once the clouds form and feedback ensues the density decreases rapidly. This is also seen in Figure 4 (top left) where we plot the cumulative density distributions at later times $T \geq T_0$ post feedback. Within 10 to 20 Myr the density distribution has decreased by around *three* orders of magnitude. Eventually, here shown at time $T = T_0 + 100$ Myr, the density distribution of the material that made up the clouds at time T_0 is indistinguishable from that of the ISM as a whole. Thus the material which makes up the clouds is fully mixed back into the ISM.

3.2 Velocity fields

In Figure 5 we plot contours of constant α superposed on the underlying density distribution at time $T_0 = 200$ Myr. Here the asymmetry between contraction and expansion timescales is apparent. There are almost no contours corresponding to contraction on a timescale of 4 Myr, corresponding to $\alpha = -0.25$, whereas there are many corresponding to expansion on that timescale. Similarly in Figure 6 there are almost no points with $\alpha < -0.25$ whereas there are many with $\alpha > 0.25$. From Figure 7 we also see that there are many dense points with $\alpha < 0$ and $|\alpha| < \beta$, indicating gravitational collapse. There are also a few regions which are converging (see contours in Figure 5) where the density is low, presumably where non gravitational effects, e.g. thermal instabilities and stochastic flows, act on the gas. However the fraction of points with $\alpha < 0$ and $|\alpha| < \beta$ is higher compared to the other calculations. Thus self gravity has a greater influence on the gas flows in this simulation.

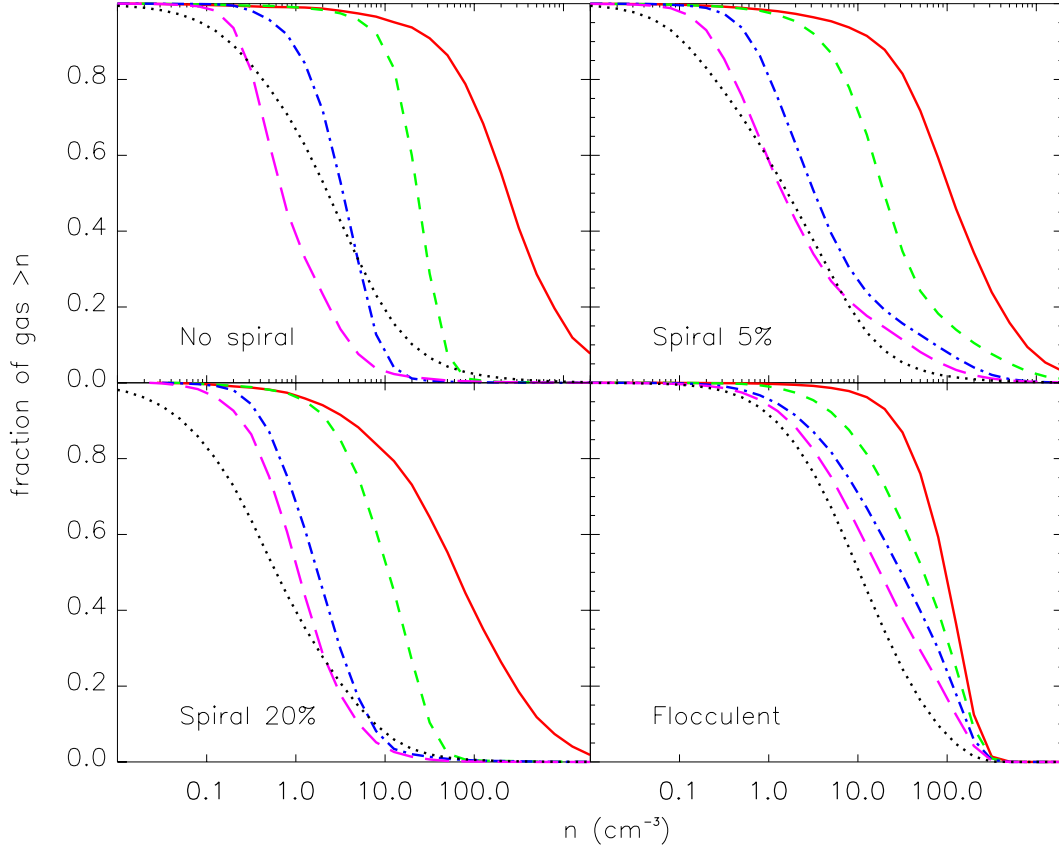


Figure 2. The cumulative distribution functions are shown for constituent gas of molecular clouds at times of $T_0 - 50$ (magenta, long dash), $T_0 - 30$ (blue, dot dash), $T_0 - 10$ (green, dash), T_0 (red, solid) Myr for the different models. The black (dotted) line shows the cdf for all the gas at a time of $T_0 - 50$ Myrs (note that the cdf for all the gas does not change significantly between $T_0 - 100$ and $T_0 + 100$ Myr). Even at $T_0 - 50$ Myr, the distribution of gas which forms the clouds is fairly atypical for the ISM of the galaxy.

4 IMPOSED SPIRAL PATTERN, 5% FEEDBACK EFFICIENCY

In this model the feedback is the same as in Section 3.1 but a spiral pattern is included in the applied stellar potential. This $m = 4$ spiral pattern is clearly apparent in the gas column density (Figure 1, top right).

4.1 Density Evolution

In Figure 2 (top right) we show the density distribution of that material which ends up in GMCs at time $T_0 = 200$ Myr for the model with a spiral potential. In contrast to the case with no superposed spiral, the distribution at time $T_0 - 50$ Myr is less different from the underlying ISM, with 80 % of the gas with $3 \text{ cm}^{-3} < n < 300 \text{ cm}^{-3}$, spanning two orders of magnitude. Prior to cloud formation the gas tends to exhibit a wider range of densities compared to the case without a spiral potential. By $T_0 - 30$ Myr however the material which will make up the clouds is distinctly atypical. The median density ($\bar{n} \approx 3 \text{ cm}^{-3}$) is about 2–3 times larger than the typical ISM. At $T_0 - 10$ Myr, the median density has increased to $\bar{n} \approx 20 \text{ cm}^{-3}$ and 80% of the material has densities in the range $3 \text{ cm}^{-3} < n < 200 \text{ cm}^{-3}$.

From Figure 4 we see that in this case the amount of

energy and momentum input as a result of star formation and feedback is not sufficient to disperse all of the dense clouds. Thus even some 100 Myr later, although the low density end of the density distribution resembles that of the ISM, some 20% of the gas that was in clouds at time T_0 still has densities above $n \geq 100 \text{ cm}^{-3}$. Thus the long-term properties of the ISM have not yet reached an equilibrium.

4.2 Velocity Field

In Figure 5 (top right), in contrast to the case considered in Section 3, the contours of $\alpha < -0.1$, that is regions contracting on timescales $\tau < 10$ My are strongly correlated with the density enhancements which we would identify as spiral arms. Regions expanding on similar timescales (that is, contours of $\alpha > 0.1$) can be found not only just downstream of the main density enhancements, but also spread throughout the interarm regions.

From Figure 6 (top right) we see that the nature of the converging flow is here quite different to the model with no spiral potential. Here asymmetry between converging and diverging flows is more pronounced. The converging flows with $\alpha < -0.1$, that is timescales $\tau < 10$ Myr, are scattered roughly around the line $|\alpha| \approx \beta$, indicating that the conver-

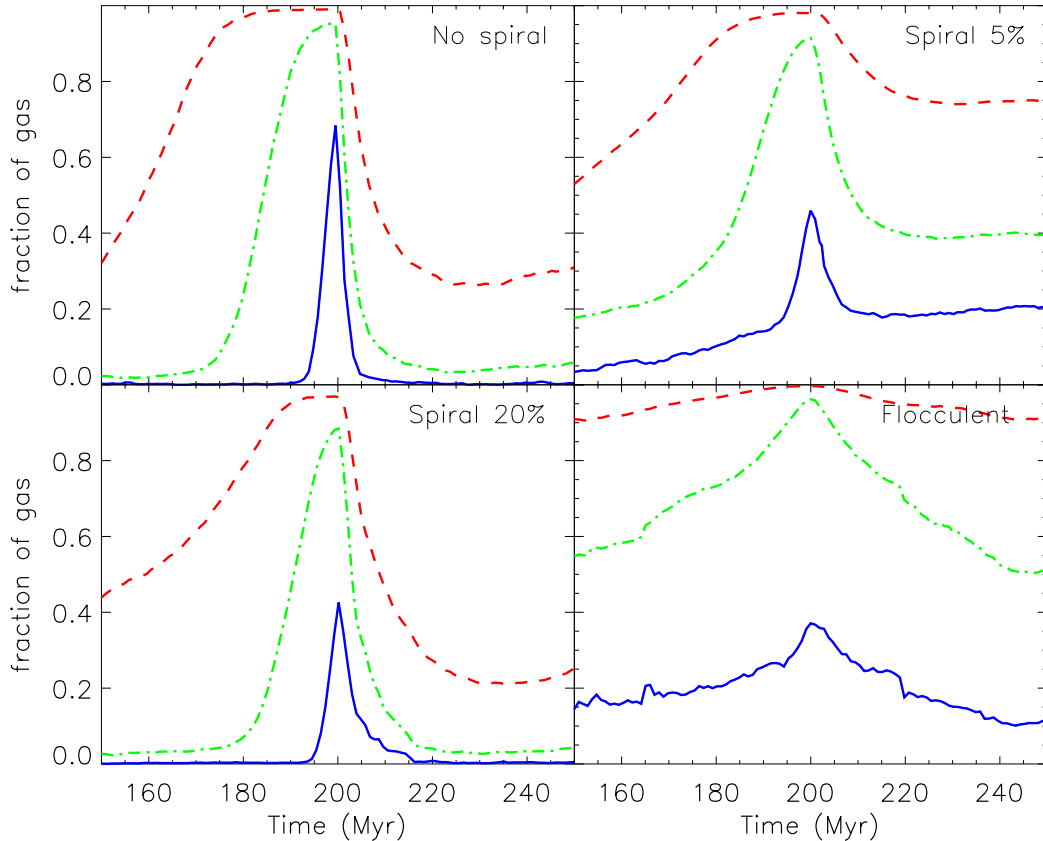


Figure 3. The fraction of gas over densities of 1 (red, dashed), 10 (green, dot dash) and 100 (blue, solid) cm^{-3} in the molecular clouds is shown versus time for the different models.

gence is mainly along one direction. Figure 7 again indicates that these points are predominantly regions of higher density, and that the spiral shocks preferentially compress gas which is already relatively dense and cold. Flows diverging on timescales $\alpha > 0.1$ fall mainly to the left of the $\alpha = \beta$ line in Figure 6 indicating that such flows are diverging in all directions.

5 IMPOSED SPIRAL PATTERN, 20% FEEDBACK EFFICIENCY

In this model the effects of feedback are so strong that the presence of the underlying spiral pattern is almost obliterated (Figure 1 lower left). Thus this model lies intermediate between the model in Section 3 which has no imposed spiral pattern and the model in Section 4 where because of the weaker feedback the imposed spiral pattern has a much stronger influence on the structure.

5.1 Density evolution

From Figure 2 (lower left) we find again that at time $T = T_0 - 50$ Myr the distribution of densities in material that will make up the GMCs at time T_0 differs from that of the average ISM. The distribution of densities is more uniform than that in the mean ISM, but is not as uniform as

that found in the gas in Section 3. The density distribution increases by a factor of about 10 between $T = T_0 - 50$ Myr and $T = T_0 - 10$ Myr. In the final 10 Myr the densities increase most rapidly, until at T_0 they span $5 \text{ cm}^{-3} < n < 500 \text{ cm}^{-3}$. After star formation and feedback occur the density of the gas that made up the clouds decreases rapidly. After 10 Myr the densities decrease by two orders of magnitude and the density distribution is essentially the same as that of the average ISM. But the material is clearly still expanding because at $T = T_0 + 30$ Myr the densities decrease further by factors of 2–3. As for the case discussed in Section 3 at time $T = T_0 + 100$ Myr, the density distribution of the material that was in the GMCs is indistinguishable from that of typical ISM material.

5.2 Velocity fields

For this case it is evident from Figure 5 (lower left) that the timescales on which both convergence and divergence occur are much shorter than in the case with lower feedback efficiency (Section 4). This is also evident in Figure 6 (lower left) where we have needed to change the scales for both α and β by a factor of 10. We also find that the regions showing most rapid convergence (contours of $\alpha < 1$, or timescales $\tau < 1$ Myr) are not as strongly correlated with density as in the case with weaker feedback (Section 4). Indeed, and

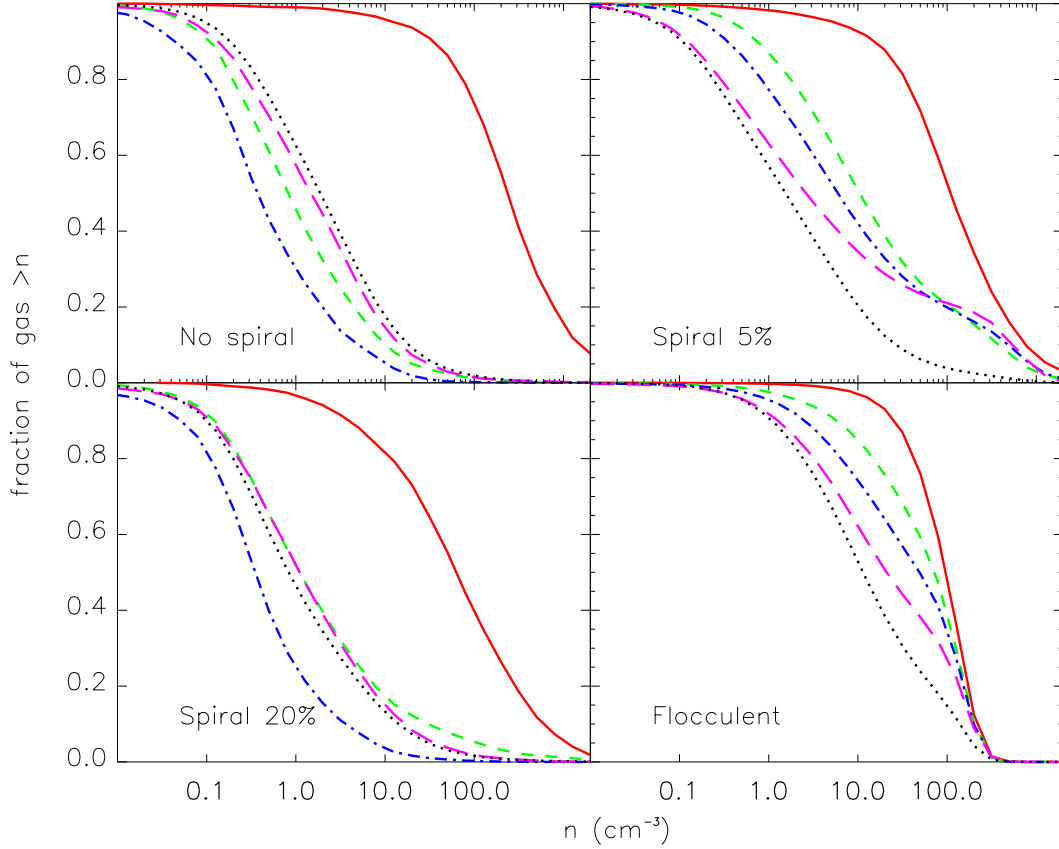


Figure 4. The cumulative distribution functions are shown for constituent gas of molecular clouds at times of T_0 (red, solid), $T_0 + 10$ (green, dash), $T_0 + 30$ (blue, dot dash), $T_0 + 100$ (magenta, long dash) Myrs for the different models. The black (dotted) line shows the cdf for all the gas at a time of $T_0 + 100$ Myrs (note that the cdf for the total ISM at $T_0 + 100$ is very similar to that at $T_0 - 50$ shown in Figure 2). By $T_0 + 100$ Myr, the gas in the clouds is indistinguishable from the ISM for the No Spiral and Spiral 20 % cases, but the gas is not fully recycled for the models with a stronger spiral component.

as also seen in Figure 7, some rapidly contracting regions seem to have very low density, although it is noticeable that these are almost always to be found next to regions of rapid expansion ($\alpha > 1$), as expected if the compression is induced by stellar feedback rather than gravity. Comparing Figure 5 (lower and upper left) it is evident that the underlying spiral potential has a much weaker effect on the dynamics of the ISM in this case. As the distribution of points in the $\alpha - \beta$ plane is independent of the gas density (Figure 7), the stellar feedback appears to be controlling the flows in the ISM regardless of density enhancements in the gas or stars.

Figure 6 (lower left) shows that all converging flows with timescales $\tau < 1$ Myr (that is, $\alpha < -1$) have $\beta \geq |\alpha|$. This implies that while these flows have strong convergence in one direction, they also display significant divergence in the perpendicular direction – like a stream of water striking a brick wall. For similar timescales ($\tau < 1$ Myr), flows that display net expansion have $\alpha > 1$. Although there are some points with $\alpha < \beta$ in the majority of cases are characterised by $\beta \geq \alpha$. This is somewhat surprising as one might imagine that strong feedback might tend to generate expansion in all directions, whereas the evidence in Figure 6 suggests that the strong net expansion is accompanied typically by contraction along one axis.

6 FLOCCULENT GALAXY, 5 % EFFICIENCY FEEDBACK

In this model, spiral structure is generated by perturbations in the stellar component, so the gas is not as structured as in the No Spiral model, but neither is there a grand design structure like the Spiral 5% model. For the flocculent galaxy, the gas surface density decreases with radius. Thus gas near the centre tends to be high surface density regardless of whether it lies in a cloud. Hence for this model we only select clouds in a torus between $r = 3.5$ and 5.5 kpc, where the average gas surface density is similar to the other models.

6.1 Density evolution

From Figure 2 (lower right), we again see that at time $T_0 - 50$ Myr, the distribution of densities differs from that of the average ISM. The distribution of material is denser than the typical ISM. At $T_0 - 50$ Myr the median density is around $n = 10 \text{ cm}^{-3}$ compared to $\bar{n} \sim 8 \text{ cm}^{-3}$ for the typical ISM. The median density increases to 50 cm^{-3} at $T_0 - 10$ Myr. There is a slightly more marked increase in density the last 10 Myrs until T_0 , although there is a lower critical density

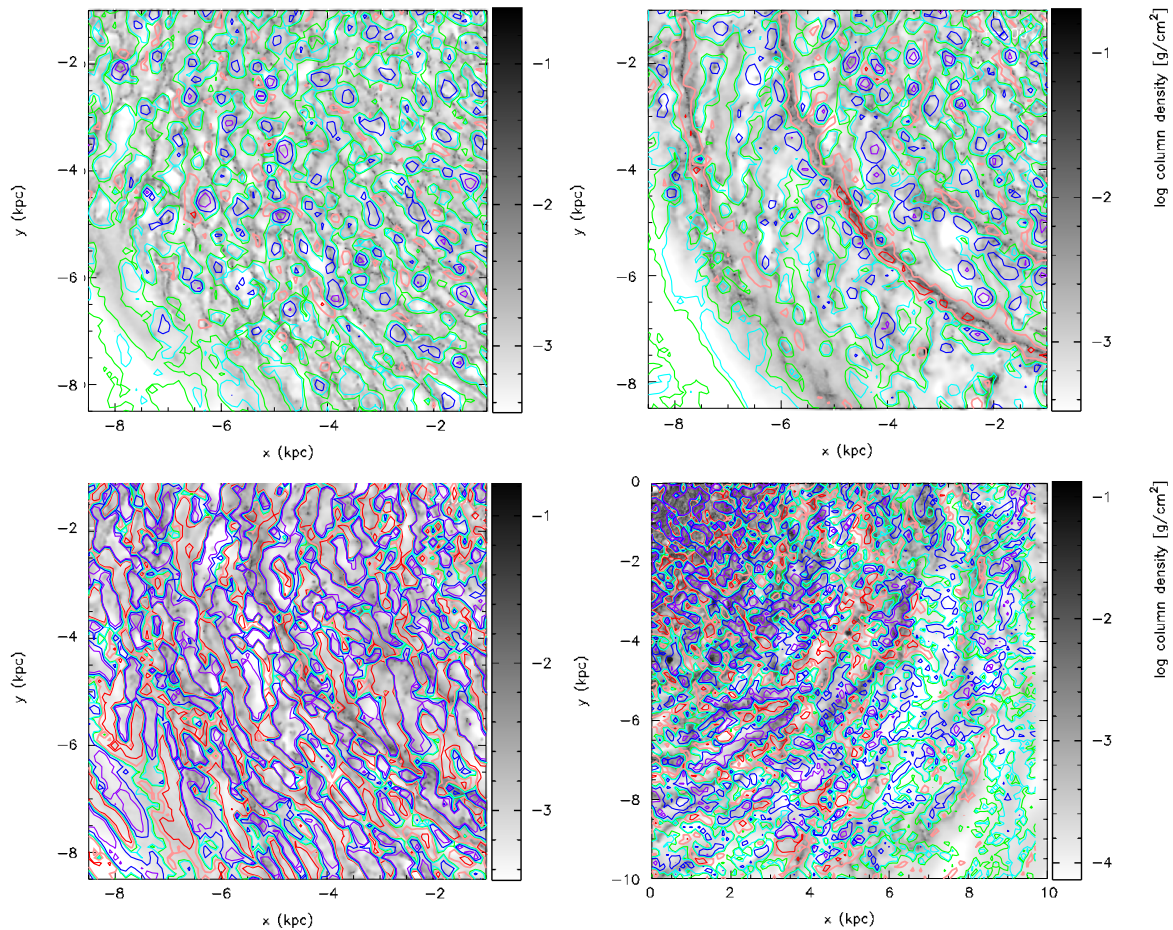


Figure 5. Contours of constant α , where α is the divergence of the velocity field, are overplotted on the column density for the No spiral (top left), Spiral 5 % (top right), Spiral 20 % (lower left) and Flocculent (lower right) models. The contours show the timescales for gas to converge or diverge. The contours represent convergence on timescales of 4 (red), 10 (orange) and 100 (green) Myr and divergence on timescales of 4 (violet), 10 (blue) and 100 (cyan) Myr. In the spiral potential model with 5 % feedback efficiency, the contours of strongest convergence clearly coincide with the spiral arms, but the patterns of convergence and divergence are much more random in the other models.

for supernovae feedback in this calculation compared to the others.

The evolution of the fraction of gas above given densities is quite different from the other simulations. There is a much higher fraction of gas above 10 and 100 cm^{-3} for the whole 100 Myr period shown in Figure 3 (lower right). In Figure 4 (lower right), we see that even after 100 Myr the material in the clouds is denser than the typical ISM. This could be because, like in the model with a spiral potential and 5 % efficiency, clouds are not disrupted by feedback. So we followed the evolution of some of the clouds in this model. We found that gas is not confined to regions the size of molecular clouds (i.e. 10's or 100's parsecs), rather the gas is much more widely spatially distributed prior to and after T_0 . However the gas does remain in spiral arms which are not disrupted. As one perturbation dissipates, the gas retains its density and then becomes part of another spiral arm. Something like this is shown in Figure 3 of Dobbs & Bonnell (2008).

We checked whether increasing the level of stellar feedback altered the density evolution in the flocculent model.

With stronger ($\epsilon = 10\%$) feedback, the gas is fully recycled, presumably the feedback is more effective in transferring dense arm material to low densities, above the plane of the disc, or in the interarm regions. The fraction of gas versus time for the clouds (Figure 3) also shows narrower peaks, and very dense ($> 100 \text{ cm}^{-3}$) gas only occurs around T_0 . Though gas with densities $> 1 \text{ cm}^{-3}$ is still overabundant compared to the other calculations.

6.2 Velocity fields

The velocity field looks somewhere in between the cases with a fixed spiral potential, and the feedback dominated case (Sections 4 and 5). Some regions of converging flows are coincident with dense spiral arms, but others are not. The distribution of α and β shows some similar characteristics to the Spiral 20% case, though the timescales are not as short. Some of the dense gas (Figure 7) exhibits $|\alpha| > \beta$ and $\alpha < 0$, indicating more uniform convergence, though similar to the Spiral 20% case, other regions of convergence are accompanied by outflows in the perpendicular direction.

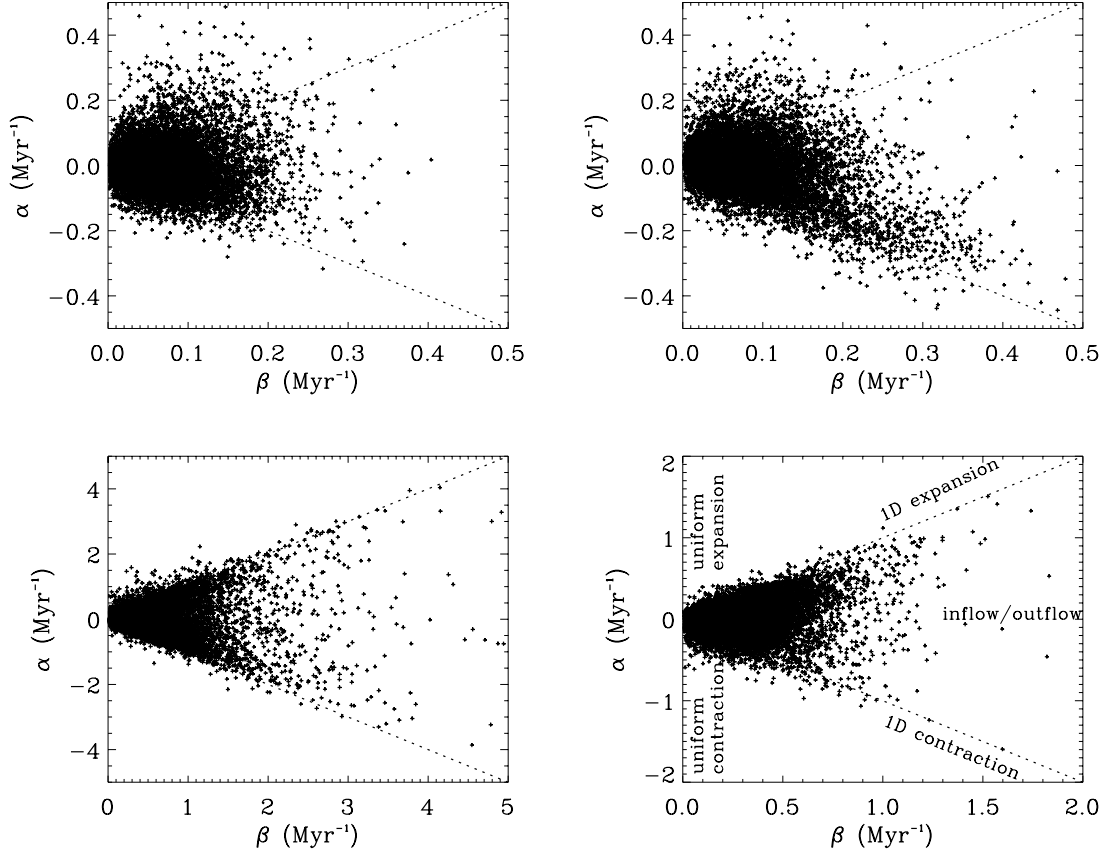


Figure 6. The values of α and β are plotted for the No spiral (top left), Spiral 5 % (top right), Spiral 20 % (lower left) and Flocculent (lower right) models. α is the divergence of the flow ($\lambda_1 + \lambda_2$), β is the difference of the eigenvalues, $|\lambda_1 - \lambda_2|$. α and β are calculated over a grid of points, with spacing 100 pc, for points between radii of 4 and 9.5 kpc. The top half of the plots correspond to expanding flows, the lower half converging. The dotted lines mark lines where $\alpha = \pm\beta$, corresponding to 1D contraction or expansion. The various regimes for the flow are marked on the last panel (for the flocculent model).

7 HIGHER RESOLUTION MODELS WITH A SPIRAL POTENTIAL

Whilst we do not have the means to rerun all our simulations at higher resolution, we did apply our analysis to a couple of higher resolution simulations, which most resemble the 5 % efficiency case with the imposed spiral potential (Section 4). We investigated the GMCs in a simulation presented by Dobbs et al. (2008), which uses 8 million particles (model 2) with a mass resolution of $312 M_\odot$ per particle. This simulation did not include self gravity or feedback, rather just the spiral potential and the thermodynamics. However the behaviour was very similar to that of the 5 % efficiency case with the imposed spiral potential (Section 4), for example the range of densities span three orders of magnitude prior to and after GMC formation. This is not so surprising since, as we discuss in the next sections, the dynamics are driven foremost by the spiral potential. The only difference is the hump apparent at higher densities in Figure 4 (top right) does not occur, as in the absence of self gravity the GMCs are always disrupted by shear, and after 100 Myr the gas is fully recycled.

Finally we also examined an unpublished calculation, which uses an $m = 2$ spiral potential, 8 million particles

(again with a mass resolution of $312 M_\odot$), which includes self gravity and feedback. Again the properties of the gas before and after GMC formation are similar to the model with 5 % efficiency and a spiral potential (see Figure 8). For both the higher resolution simulations, the gas is atypical ISM at least 30 Myr prior to and after GMC formation.

8 COMPARISON OF MODELS WITH THEORIES OF THE ISM

To make a molecular cloud it is necessary to gather a sufficient quantity of gas from the interstellar medium into a small enough volume. The questions we have attempted to address in this paper are:

- (i) which parts of the ISM are gathered together, and
- (ii) what mechanism(s) enable this to happen?

We stress again that in this paper we have concentrated on only massive ($> 10^5 M_\odot$) GMCs. Although lower mass clouds may form in similar ways, we cannot conclude anything about lower mass clouds from our results. We also note that we have not included magnetic fields in our analysis.

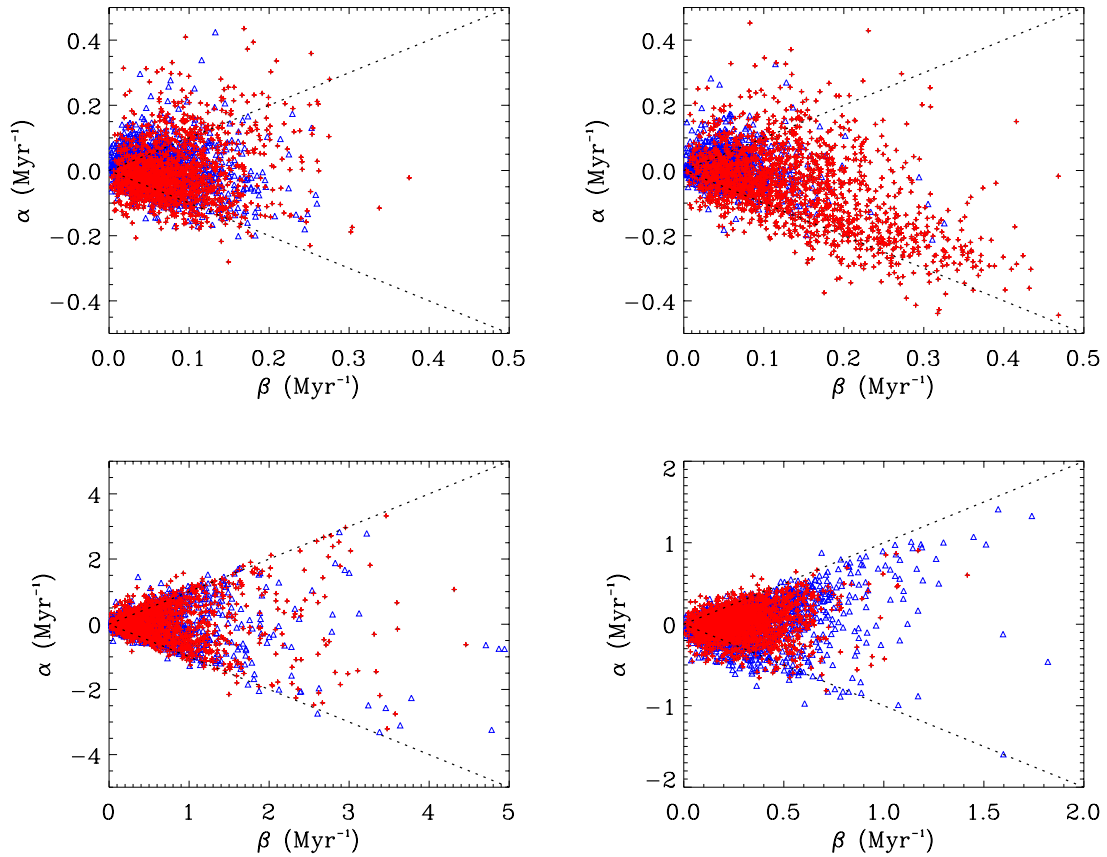


Figure 7. The values of α and β are plotted as for Figure 6 except we only show the top 10% most dense points (red crosses) and the 10% least dense points (blue triangles).

8.1 From what gas do molecular clouds form ...

Many models of molecular cloud formation start with an ISM which is uniform in density, with a density appropriate to the mean density of the ISM as a whole (typically $\bar{n} \sim 1 \text{ cm}^{-3}$; e.g. Elmegreen 1991; Kim et al. 2002; Kim & Ostriker 2006; Heitsch et al. 2006) and then investigate instabilities of various kinds (thermal, gravitational, magneto-dynamic). In contrast, Pringle et al. (2001) argued that it is difficult to form GMCs from such low density material on the necessary timescales (of order $\sim 5 - 10 \text{ Myr}$), and that the gas from which GMCs form must already be dense – within an order of magnitude of the mean cloud density, and much denser than the mean for the ISM. Pringle et al. (2001) then made the (tacit) assumption that GMCs form from typical ISM material and concluded that a large fraction of the ISM must consist of dense, possibly molecular, gas.

From our simulations it is evident that neither of these scenarios is fully correct. In each of our simulations the material which forms GMCs is significantly denser than the mean ISM by 10 Myr before cloud formation takes place (Figure 2). Thus the simple argument made by Pringle et al. (2001) is validated, and models which try to form GMCs on short timescales from gas with low average ISM densities are not likely to succeed. However, the tacit assumption made by Pringle et al. (2001) that clouds form from typical ISM material is not sustained. Indeed (Figure 2) at least

30 Myr, and in some cases 50 Myr, before cloud formation takes place, the density distribution of the material destined to be part of GMCs differs significantly from the average for that of the ISM as a whole.

8.2 ... and which mechanism, or mechanisms, gather it together?

The interstellar gas in galaxies is characterised by a highly inhomogeneous, turbulent and multiphase medium. A number of mechanisms give rise to this of which the dominant ones are:

(i) *Thermal effects.* It has long been noted (e.g. McKee & Ostriker 1977; Burkert & Lin 2000) that the ISM is a multiphase medium and that this is at least in part due to the complexity and multi-valued nature of the cooling functions. Such a structure is likely to be non-steady. As gas enters the cool phase it becomes denser and so contracts, and as it enters a warm or hot phase it expands. Thus such a structure of necessity gives rise to internal flows (Elphick et al. 1991, 1992; see the discussion in Pringle & King (2007), Chap. 8).

(ii) *Feedback.* McKee & Ostriker (1977) postulated that the multiphase nature of the ISM is regulated predominantly by supernova explosions, and indeed it is such events that we

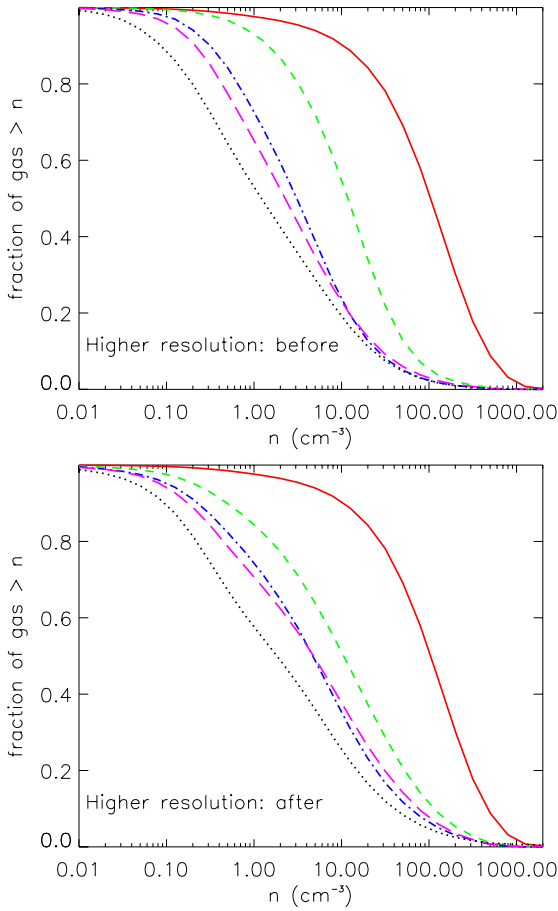


Figure 8. The cumulative distribution functions are shown for gas from a simulation with an imposed spiral potential and 8 million particles. The upper and lower panels show the constituent gas from GMCs selected at 200 Myr, at earlier and later times. The colour / line types for the upper and lower panels are the same as Figures 2 and 4 respectively.

have in mind when we insert star-formation induced feedback into our simulations.

(iii) *Self-gravity.* Although it has been established (Dobbs et al. 2006) that self-gravity is *not* necessary for the formation of GMCs, and although it is apparent that many, if not most, GMCs are not self-gravitating as a whole (Heyer et al. 2009; Dobbs et al. 2011b) it is clear that self-gravity must play a role at least in the denser parts of the GMCs in which star formation is occurring, and also helps form more massive GMCs (Kwan & Valdes 1987; Dobbs 2008).

(iv) *Non-axisymmetries in the underlying stellar potential.* If the underlying stellar potential is non-axisymmetric, non-circular perturbations will be induced in the velocity field. These can give rise to shocks, especially in the higher density, cooler component of the ISM. We consider two cases (i) a steady spiral potential with fixed pattern speed, to mimic global tidally induced spiral structure (e.g. M 51) and, (ii) a model in which the underlying stellar component is gravitationally unstable, to model flocculent galaxies (cf. Wada et al. 2011).

We have analysed the local, vertically-averaged velocity flows in our simulations by considering the eigenvalues, λ_1, λ_2 of the two-dimensional rate of strain tensor, e_{ij} , on a size scale of 100 pc (Figures 5 and 6). Plots of the divergence $\alpha = \lambda_1 + \lambda_2 = \nabla \cdot \mathbf{u}$ versus $\beta = |\lambda_1 - \lambda_2|$ are given in Figure 6. In this Figure each point represents the nature of the flow locally at a position in the model. The area of this Figure in which points lie at larger values of $|\alpha|$ (shorter timescales) tells us about the nature of the flows which are contracting ($\alpha < 0$) or expanding ($\alpha > 0$) the most rapidly. As discussed already, points which best approximate 1D colliding flows (often adopted as initial conditions for molecular cloud formation, e.g. Heitsch et al. 2006; Banerjee et al. 2009; Vázquez-Semadeni et al. 2011) exhibit $\alpha \approx -\beta$. Unsurprisingly, all our models contain some points which satisfy this criterion. However only the Spiral 5% model preferentially contains flows which are of this nature.

For the No Spiral case (Section 3), the random motions in the ISM are induced by a combination of thermal effects, feedback and self-gravity. We find that the rapidly contracting flows (timescales < 4 Myr) do so more uniformly (i.e. have more points for which both $\lambda_1 < 0$ and $\lambda_2 < 0$) than for the other cases, especially for the denser gas (Figure 7). This seems to imply that in this case self-gravity plays a strong, but not always a dominant, role in the final gathering of material as it forms a GMC.

As mentioned above, for the case of a superimposed spiral with moderate feedback (Spiral 5%, Section 4), the rapidly contracting flows lie preferentially along the line $\alpha \approx -\beta$ indicating that the final contraction occurs predominantly in the one-dimensional manner. This is not a surprise since the shock induced by the spiral potential will tend to produce a one-dimensional compressional flow. We have remarked above that the cloud formation process differs here from that usually assumed because the density of the material is much higher than the mean ISM density. It is worth noting here that it is the cooler, denser component (say, molecular) of the ISM which undergoes the stronger shock and so undergoes the greater degree of compression (Figure 7). This is evidenced by the fact that the high density gas has much larger eigenvalues ($|\lambda_1|, |\lambda_2|$) in Figure 7 than the low density gas.

In the same superimposed spiral potential, but with much stronger feedback (Spiral 20%, Section 5), the feedback is sufficiently energetic that the non-axisymmetric effects of the potential are to some extent overwhelmed (Figures 1 and 5). If, in Figure 6, we compare this case with the Spiral 5% case, we note that the flow timescales are here much shorter. This must imply that in this case the internal motions of the ISM are dominated by feedback, as anticipated by McKee & Ostriker (1977) and modelled by many authors (Rosen & Bregman 1995; de Avillez & Breitschwerdt 2004; Slyz et al. 2005; Joung & Mac Low 2006). The points in Figure 6 lie almost entirely within the region $\beta \geq |\alpha|$, implying that the local flows are highly non-uniform, with a large velocity in one direction (expansion or compression) together with a smaller, but usually non-negligible, velocity of the *opposite sign* in the perpendicular direction (similar to the colliding flows models of Audit & Hennebelle (2005) which employ open boundary conditions). The lack of the strong correlation between rapidly converging flows (regions of large, negative α in Figure 5) and the local density (con-

firmed by the fact that the low and high density points in Figure 7 are similarly distributed in the (α, β) -plane implies that it is indeed strong feedback which is the main driver.

The behaviour of the ISM subject to a ‘live’ stellar disc (‘Flocculent’, Section 6), in which the stellar arms are non-steady, forming and then being wound and stretched by galactic shear, has been modelled by a number of authors (Li et al. 2005; Dobbs & Bonnell 2007; Robertson & Kravtsov 2008; Dobbs & Pringle 2009; Hopkins et al. 2011; Wada et al. 2011). The local stellar densities in the arms change typically on an orbital timescale (say, ~ 100 Myr) and there is a tendency for the arms to bifurcate and/or to merge with other arms. In Figures 5 and 6 we see that the timescales on which the local gas density changes is often much shorter than this, e.g. $\tau > 0.2$ corresponding to a timescale of < 5 Myr. Here again (Figure 6) most, but not all, of the points have $|\alpha| \leq \beta$, so again often contraction in one direction is accompanied by expansion in the other (through feedback and/or shear).

9 CONCLUSIONS

We have investigated models for the formation of molecular clouds which encompass most of the physical mechanisms usually envisaged, including predominantly self-gravity (No Spiral), compressive shocks in a spiral arm (Spiral 5%), feedback from supernovae (Spiral 20%) and flow subject to non-steady potential minima in a ‘live’ stellar disc (Flocculent). All these mechanisms are capable of forming molecular clouds and it is of interest to try to determine which (if any) dominates in a particular galaxy. A related question is whether the timescales for cloud formation and dispersal, and the nature of the ISM which goes into making up clouds, differ in these different scenarios.

Whilst we generally see a transition from predominantly low to high densities when GMCs form (e.g. from atomic to molecular gas), this transition occurs over a long (10’s of Myrs) time period. Thus our main finding is that GMCs do not form from typical or average interstellar material. At 30 Myr, and in some cases even 50 Myr before cloud formation, the density distribution of the cloud-forming material differs significantly from that of the ISM as a whole. Within 10 Myr prior to cloud formation the mean density of gas destined to make up a cloud is within an order of magnitude of mean density of the cloud. Given the strongly inhomogeneous nature of the ISM, whatever the mechanism which gathers material together – whether it depends strongly on density (e.g. self-gravity) or not (e.g. supernova explosions) – it is that material which is already of higher density that is more likely to form the GMCs (Pringle et al. 2001).

We find that in most cases the effect of feedback is to fully recycle material to the ISM (Figure 4). The exceptions to this are the self-gravitating long-lived entities which form in Spiral 5% model, and the clouds in the spiral arms of the Flocculent model. Both of these simulations are characterised by a clear spiral structure and a lower level of feedback. In these models, it appears (Figure 4) that material which forms GMCs has a tendency to remain denser than average. This raises the possibility that the abundances of gas to be found within star-forming regions (i.e. dense clouds

and flocculent spiral arms) might differ significantly from the abundances of gas in the ambient ISM.

We also find (Figures 5, 6 and 7) that the nature of small-scale flows within the ISM can give strong clues as to the nature of the dominant mechanism by which GMCs are formed in a particular galaxy. For example a comparison of the distributions of points in Figures 6 and 7 for the Spiral 5% and the Flocculent models, both of which have similar levels of feedback, indicates a significant difference between models of spiral galaxies in which the gas flows relative to the arm pattern (as in density wave theory) or in which the pattern and circular flow essentially co-rotate (see also Wada et al. 2011). Likewise, a comparison between the models which form GMCs predominantly due to self-gravity of the gas (No Spiral) and which form GMCs predominantly due to the self-gravity of the underlying stellar component (Flocculent), both of which present a ‘flocculent’ appearance, shows that the groupings of points within the (α, β) -plane are easily distinguishable. Lastly, our model where the gas flows are dominated by stellar feedback (Spiral 20%) exhibits different characteristics again compared to the other simulations. With future facilities, such as ALMA, such comparisons can become reality.

10 ACKNOWLEDGMENTS

We thank an anonymous referee for a helpful report which improved the paper. CLD acknowledges funding from the European Research Council for the FP7 ERC starting grant project LOCALSTAR. JEP thanks Exeter University for funding visits to the Exeter Astrophysics group. Calculations were performed on facilities at Garching, and the University of Exeter Supercomputer, a DiRAC Facility jointly funded by STFC, the Large Facilities Capital Fund of BIS, and the University of Exeter. Figure 1 was produced using SPLASH (Price 2007).

REFERENCES

- Audit E., Hennebelle P., 2005, *A&A*, 433, 1
- Ballesteros-Paredes J., Hartmann L., Vázquez-Semadeni E., 1999, *ApJ*, 527, 285
- Banerjee R., Vázquez-Semadeni E., Hennebelle P., Klessen R. S., 2009, *MNRAS*, 398, 1082
- Burkert A., Lin D. N. C., 2000, *ApJ*, 537, 270
- Cox D. P., Gómez G. C., 2002, *ApJS*, 142, 261
- de Avillez M. A., Breitschwerdt D., 2004, *A&A*, 425, 899
- Dib S., Bell E., Burkert A., 2006, *ApJ*, 638, 797
- Dobbs C. L., 2008, *MNRAS*, 391, 844
- Dobbs C. L., Bonnell I. A., 2006, *MNRAS*, 367, 873
- Dobbs C. L., Bonnell I. A., 2007, *MNRAS*, 374, 1115
- Dobbs C. L., Bonnell I. A., 2008, *MNRAS*, 385, 1893
- Dobbs C. L., Bonnell I. A., Pringle J. E., 2006, *MNRAS*, 371, 1663
- Dobbs C. L., Burkert A., Pringle J. E., 2011a, *MNRAS*, 417, 1318
- Dobbs C. L., Burkert A., Pringle J. E., 2011b, *MNRAS*, 413, 2935
- Dobbs C. L., Glover S. C. O., Clark P. C., Klessen R. S., 2008, *MNRAS*, 389, 1097

- Dobbs C. L., Pringle J. E., 2009, MNRAS, 396, 1579
- Dobbs C. L., Theis C., Pringle J. E., Bate M. R., 2010, MNRAS, 403, 625
- Elmegreen B. G., 1991, ApJ, 378, 139
- Elphick C., Regev O., Shaviv N., 1992, ApJ, 392, 106
- Elphick C., Regev O., Spiegel E. A., 1991, MNRAS, 250, 617
- Field G. B., Saslaw W. C., 1965, ApJ, 142, 568
- Gibson S. J., 2010, in R. Kothes, T. L. Landecker, & A. G. Willis ed., *Astronomical Society of the Pacific Conference Series Vol. 438 of Astronomical Society of the Pacific Conference Series, Cold Atomic Gas in the CGPS and Beyond*. pp 111–+
- Gibson S. J., Taylor A. R., Higgs L. A., Brunt C. M., Dewdney P. E., 2005, ApJ, 626, 195
- Glover S. C. O., Mac Low M.-M., 2007, ApJS, 169, 239
- Gressel O., Elstner D., Ziegler U., Rüdiger G., 2008, A&A, 486, L35
- Heitsch F., Hartmann L., 2008, ApJ, 689, 290
- Heitsch F., Slyz A. D., Devriendt J. E. G., Hartmann L. W., Burkert A., 2006, ApJ, 648, 1052
- Hennebelle P., Banerjee R., Vázquez-Semadeni E., Klessen R. S., Audit E., 2008, A&A, 486, L43
- Heyer M., Krawczyk C., Duval J., Jackson J. M., 2009, ApJ, 699, 1092
- Hopkins P. F., Quataert E., Murray N., 2011, MNRAS, 417, 950
- Joung M. K. R., Mac Low M.-M., 2006, ApJ, 653, 1266
- Kim W., Ostriker E. C., Stone J. M., 2002, ApJ, 581, 1080
- Kim W.-T., Ostriker E. C., 2006, ApJ, 646, 213
- Koyama H., Inutsuka S., 2000, ApJ, 532, 980
- Kuijken K., Dubinski J., 1995, MNRAS, 277, 1341
- Kwan J., Valdes F., 1987, ApJ, 315, 92
- Leisawitz D., Bash F., 1982, ApJ, 259, 133
- Li Y., Mac Low M.-M., Klessen R. S., 2005, ApJ, 626, 823
- McKee C. F., Ostriker J. P., 1977, ApJ, 218, 148
- Monje R. R., Emprechtinger M., Phillips T. G., Lis D. C., Goldsmith P. F., Bergin E. A., Bell T. A., Neufeld D. A., Sonnentrucker P., 2011, ApJL, 734, L23+
- Ntormousi E., Burkert A., Fierlinger K., Heitsch F., 2011, ApJ, 731, 13
- Pagani L., Roueff E., Lesaffre P., 2011, ApJL, 739, L35+
- Price D. J., 2007, *Publications of the Astronomical Society of Australia*, 24, 159
- Pringle J. E., Allen R. J., Lubow S. H., 2001, MNRAS, 327, 663
- Pringle J. E., King A. R., 2007, *Astrophysical flows*
- Roberts W. W., Stewart G. R., 1987, ApJ, 314, 10
- Robertson B. E., Kravtsov A. V., 2008, ApJ, 680, 1083
- Rosen A., Bregman J. N., 1995, ApJ, 440, 634
- Shetty R., Ostriker E. C., 2006, ApJ, 647, 997
- Slyz A. D., Devriendt J. E. G., Bryan G., Silk J., 2005, MNRAS, 356, 737
- Strasser S. T., Dickey J. M., Taylor A. R., Boothroyd A. I., Gaensler B. M., Green A. J., Kavars D. W., Lockman F. J., Martin P. G., McClure-Griffiths N. M., Rothwell T. A., Stil J. M., 2007, AJ, 134, 2252
- Tasker E. J., 2011, ApJ, 730, 11
- Tasker E. J., Tan J. C., 2009, ApJ, 700, 358
- Tomisaka K., 1984, PASJ, 36, 457
- Tomisaka K., 1986, PASJ, 38, 95
- Vázquez-Semadeni E., Banerjee R., Gómez G. C., Hennebelle P., Duffin D., Klessen R. S., 2011, MNRAS, 414, 2511
- Vázquez-Semadeni E., Gómez G. C., Jappsen A. K., Ballesteros-Paredes J., González R. F., Klessen R. S., 2007, ApJ, 657, 870
- Wada K., Baba J., Saitoh T. R., 2011, ApJ, 735, 1
- Wada K., Spaans M., Kim S., 2000, ApJ, 540, 797

This paper has been typeset from a \LaTeX file prepared by the author.